

# yambo: an *ab initio* tool for excited state calculations

Andrea Marini<sup>a,e,1</sup>, Conor Hogan<sup>b,e</sup>, Myrta Grüning<sup>c,e</sup>, and Daniele Varsano<sup>d,e</sup>

<sup>a</sup> *Dipartimento di Fisica, CNISM, and SMC Institute for Statistical Mechanics and Complexity, Università di Roma “Tor Vergata”, Via della Ricerca Scientifica 1, I-00133 Roma, Italy*

<sup>b</sup> *Dipartimento di Fisica and INFN-CNR, Università di Roma “Tor Vergata”, Via della Ricerca Scientifica 1, I-00133 Roma, Italy*

<sup>c</sup> *Unité PCPM, Université Catholique de Louvain, 1348 Louvain-la-Neuve, Belgium*

<sup>d</sup> *National Center on nanoStructures and Biosystems at Surfaces (S3) of INFN-CNR, I-41100 Modena, Italy*

<sup>e</sup> *European Theoretical Spectroscopy Facility (ETSF)*

## Abstract

**yambo** is an *ab initio* code for calculating quasiparticle energies and optical properties of electronic systems within the framework of many-body perturbation theory and time-dependent density functional theory. Quasiparticle energies are calculated within the *GW* approximation for the self-energy. Optical properties are evaluated either by solving the Bethe–Salpeter equation or by using the adiabatic local density approximation. **yambo** is a plane-wave code that, although particularly suited for calculations of periodic bulk systems, has been applied to a large variety of physical systems. **yambo** relies on efficient numerical techniques devised to treat systems with reduced dimensionality, or with a large number of degrees of freedom. The code has a user-friendly command-line based interface, flexible I/O procedures and is interfaced to several publicly available density functional ground-state codes.

PACS: 71.35.-y, 71.15.-m, 71.45.Gm, 71.15.Qe

*Key words:* Electronic structure; optical properties; excitons; quasiparticles;

## PROGRAM SUMMARY

*Program title:* **yambo**

*Journal Reference:*

*Catalogue identifier:*

*Program obtainable from:* <http://www.yambo-code.org>

*Licensing provisions:* This program is distributed under the GNU General Public License v2.0 ( see <http://www.gnu.org/> for details)

*Programming language:* Fortran 95, C

*Computer(s) for which the program has been designed:* any computer architecture, running any flavor of UNIX

<sup>1</sup> Corresponding author

*Operating system(s) under which the program has been tested:* GNU/Linux, AIX, Irix, OS/X

*RAM required to execute program with typical data:* 10–1000 Mbytes

*Number of processors used:* Up to 100

*Supplementary material:* Manuals, tutorials, background theory and sample input files are available for download or inspection from the website <http://www.yambo-code.org>

*Keywords:* many-body perturbation theory, density functional theory, time-dependent density functional theory, self-energy, Bethe-Salpeter equation, excitons, quasiparticles, plasmons

*PACS:* 71.35.-y, 71.15.-m, 71.45.Gm, 71.15.Qe

*Classification:* 7.3 Electronic Structure, 4.4 Feynman Diagrams, 7.2 Electron Spectroscopies, 18 Optics

*External routines/libraries:*

- BLAS (<http://www.netlib.org/blas/>)
- LAPACK (<http://www.netlib.org/lapack/>)
- MPI ([www-unix.mcs.anl.gov/mpi/](http://www-unix.mcs.anl.gov/mpi/)) is optional.
- BLACS (<http://www.netlib.org/scalapack/>) is optional.
- SCALAPACK (<http://www.netlib.org/scalapack/>) is optional.
- FFTW (<http://www.fftw.org/>) is optional.
- netCDF ([www.unidata.ucar.edu/software/netcdf/](http://www.unidata.ucar.edu/software/netcdf/)) is optional.

*Nature of problem:*

Calculation of excited state properties (quasiparticles, excitons, plasmons) from first principles.

*Solution method:*

Many body perturbation theory (Dyson equation, Bethe–Salpeter equation) and time-dependent density functional theory. Quasiparticle approximation. Plasmon-pole model for the dielectric screening. Plane-wave basis set with norm conserving pseudopotentials.

*Unusual features:*

During execution, **yambo** supplies estimates of the elapsed and remaining time for completion of each runlevel. Very friendly shell-based user-interface.

*Additional comments:*

**yambo** was known as “SELF” prior to GPL release. It belongs to the suite of codes maintained and used by the European Theoretical Spectroscopy Facility (ETSF) [1]

*Running time:*

The typical **yambo** running time can range from a few minutes to some days depending on the chosen level of approximation, and on the property and physical system under study.

## LONG WRITE-UP

### 1. Introduction

*Ab initio* calculations in the framework of density functional theory (DFT) [2] have yielded high-quality results for a large variety of systems, ranging from periodic solids to molecules and nanostructures [2]. These results are however mostly limited to quantities related to the electronic *ground state*, whereas additional phenomena that occur in the excited state are not correctly described [3].

It was recognized at an early stage [4] that in extended systems the standard approximations for DFT – the local density (LDA) or generalized gradient (GGA) approximations – fail to describe, among other effects, the band gap of insulators and semiconductors [3]. In contrast, many-body perturbation theory (MBPT) [5] provides, by means of the quasiparticle (QP) concept, a more adequate and accurate approach that yields band gaps (and band structures, in general) in good agreement with the experimental values [3].

While the first successful QP calculations were performed in the mid 80’s [6], it was only in the late 90’s that many-body effects have been included in the *ab initio* calculation of optical properties of real materials [7]. It is now well known that a quantitative description of the optical response of an interacting electron system must account for electron–hole interactions (excitonic effects) [3]. This is achieved by solving the Bethe–Salpeter (BS) equation for the electron–hole Green’s function, within the MBPT framework. Nowadays, solving the BS equation is the state-of-the-art approach for calculating optical properties in extended systems. The importance of including excitonic effects is clear on comparison with the experimental absorption spectra of semiconductors and insulators. In particular, for wide-gap insulators there is hardly any resemblance between the spectrum calculated within a noninteracting theory and the experiment.

An alternative approach to the study of correlation in many-body systems is given by time dependent DFT (TDDFT) [8]. Similar to the paradigm of DFT for ground-state properties, TDDFT has emerged as a very powerful tool for the description of excited states. In principle TDDFT is an exact theory for neutral excited state properties. Nevertheless, in practice it has a number of commonly cited failures related to the approximation of the exchange–correlation (xc) kernel. One example is the difficulty encountered when studying the optical properties of extended systems; another is the severe underestimation of high-lying excitation energies in molecules. On the other hand, the combination of TDDFT with simple approximations for the xc kernel (based on the homogeneous electron gas) has been successfully applied to the study of the optical response of molecules and nanostructures.

Quasiparticles, excitons and plasmons are the excitations that can be calculated using the `yambo` code. These excitations are ubiquitous in the *ab initio* description of the electronic and optical properties of any physical system. The `yambo` code uses as input the result of standard DFT calculations obtained by means of publicly available codes [9,10]. The theoretical tools implemented in `yambo` are TDDFT and the BS equations for the response function and the Dyson equation in the *GW* approximation for the QPs.

The paper is structured as follows. In Section 2 we introduce the most important theoretical concepts as they are utilized in `yambo`, before describing some of the most important numerical algorithms implemented in the code in Section 3. Section 4 outlines the structure and capabilities of `yambo`. A more detailed description of how the code is actually utilized is presented in Section 5, before some brief notes regarding installation in Section 6. Finally, an illustrative example of a typical `yambo` calculation is outlined in Section 7.

## 2. Theoretical background

### 2.1. Quasiparticles: the plasmon-pole approximation

MBPT is a rigorous approach based on the Green’s function method, and provides a proper framework for accurately computing excited state properties. For details of the Green’s function formalism and many-body techniques applied to condensed matter, we refer the reader to several comprehensive papers in the literature [5,11]. Here we shall just present some of the main equations used for the quasiparticle and optical spectra calculations.

The basic component of a many-body perturbative expansion is the reference noninteracting system, that in `yambo` is represented by the solution of the DFT Kohn–Sham (KS) equations. In the following we will label these single particle levels as  $|n\mathbf{k}\rangle$ ,  $n$  being the band index and  $\mathbf{k}$  the generic vector of the grid used to sample the Brillouin Zone (BZ). In this basis the noninteracting Green’s function  $G^0$  takes the form

$$G_{n\mathbf{k}}^0(\omega) = \frac{f_{n\mathbf{k}}}{\omega - \varepsilon_{n\mathbf{k}} - i0^+} + \frac{1 - f_{n\mathbf{k}}}{\omega - \varepsilon_{n\mathbf{k}} + i0^+}, \quad (1)$$

$f_{n\mathbf{k}}$  being the occupation factor and  $\varepsilon_{n\mathbf{k}}$  the KS energies. The basic relation between  $G^0$  and the exact Green's function is given by the Dyson equation

$$G_{n\mathbf{k}}(\omega) = \left[ (G_{n\mathbf{k}}^0(\omega))^{-1} - \Sigma_{n\mathbf{k}}(\omega) + V_{n\mathbf{k}}^{\text{xc}} \right]^{-1}, \quad (2)$$

where the contribution due to the DFT exchange-correlation potential  $V_{n\mathbf{k}}^{\text{xc}}$  is removed from the single-particle energies appearing in  $G_{n\mathbf{k}}^0(\omega)$  in order to prevent double counting of correlation effects induced by the self-energy  $\Sigma$ . Since the basic physical process that distinguishes a bare particle from a quasiparticle is the screening of the particle by means of the polarization of the surrounding medium, **yambo** uses the *GW* approximation for the electronic self-energy  $\Sigma$  [12] which is diagrammatically depicted in Fig. 1. In this approximation the self-energy is a function of  $G^0$  and of the inverse dynamical dielectric function  $\epsilon^{-1}(\mathbf{r}_1, \mathbf{r}_2; \omega)$ , and it is composed of an exchange (x), and of a correlation (c) part,

$$\Sigma_{n\mathbf{k}}(\omega) = \Sigma_{n\mathbf{k}}^x + \Sigma_{n\mathbf{k}}^c(\omega). \quad (3)$$

The exchange part is simply the Fock term of the Hartree-Fock self-energy, and it can be rewritten as

$$\Sigma_{n\mathbf{k}}^x = \langle n\mathbf{k} | \Sigma^x(\mathbf{r}_1, \mathbf{r}_2) | n\mathbf{k} \rangle = - \sum_m \int_{BZ} \frac{d\mathbf{q}}{(2\pi)^3} \sum_{\mathbf{G}} v(\mathbf{q} + \mathbf{G}) |\rho_{nm}(\mathbf{k}, \mathbf{q}, \mathbf{G})|^2 f_{m(\mathbf{k}-\mathbf{q})}, \quad (4)$$

where  $\rho_{nm}(\mathbf{k}, \mathbf{q}, \mathbf{G}) = \langle n\mathbf{k} | e^{i(\mathbf{q}+\mathbf{G})\cdot\mathbf{r}} | m\mathbf{k} - \mathbf{q} \rangle$ ,  $\mathbf{G}$  are the reciprocal lattice vectors, and  $v(\mathbf{q} + \mathbf{G}) \equiv 4\pi/|\mathbf{q} + \mathbf{G}|^2$ . The correlation part of the self-energy is given by

$$\Sigma_{n\mathbf{k}}^c(\omega) = \langle n\mathbf{k} | \Sigma^c(\mathbf{r}_1, \mathbf{r}_2; \omega) | n\mathbf{k} \rangle = i \sum_m \int_{BZ} \frac{d\mathbf{q}}{(2\pi)^3} \sum_{\mathbf{G}, \mathbf{G}'} \frac{4\pi}{|\mathbf{q} + \mathbf{G}|^2} \rho_{nm}(\mathbf{k}, \mathbf{q}, \mathbf{G}) \rho_{nm}(\mathbf{k}, \mathbf{q}, \mathbf{G}') \times \int d\omega' G_{m\mathbf{k}-\mathbf{q}}^0(\omega - \omega') \epsilon_{\mathbf{G}\mathbf{G}'}^{-1}(\mathbf{q}, \omega'). \quad (5)$$

The energy integral entering Eq.(5) can be solved once the inverse dielectric function is known. The equation of motion for  $\epsilon^{-1}$  follows from that of the reducible response function  $\chi$  [11] as

$$\epsilon_{\mathbf{G}\mathbf{G}'}^{-1}(\mathbf{q}, \omega) = \delta_{\mathbf{G}\mathbf{G}'} + v(\mathbf{q} + \mathbf{G}) \chi_{\mathbf{G}\mathbf{G}'}(\mathbf{q}, \omega). \quad (6)$$

The *GW* approximation for the self-energy is obtained when  $\chi$  is calculated within the random phase approximation (RPA) [11]

$$\chi_{\mathbf{G}\mathbf{G}'}(\mathbf{q}, \omega) = \left[ \delta_{\mathbf{G}\mathbf{G}''} - v(\mathbf{q} + \mathbf{G}'') \chi_{\mathbf{G}\mathbf{G}''}^0(\mathbf{q}, \omega) \right]^{-1} \chi_{\mathbf{G}''\mathbf{G}'}^0(\mathbf{q}, \omega). \quad (7)$$

The noninteracting response function is easily calculated in terms of the bare Green's function  $G_0$ :

$$\chi_{\mathbf{G}\mathbf{G}'}^0(\mathbf{q}, \omega) = 2 \sum_{nn'} \int_{BZ} \frac{d\mathbf{k}}{(2\pi)^3} \rho_{n'\mathbf{k}}^*(\mathbf{q}, \mathbf{G}) \rho_{n\mathbf{k}}(\mathbf{q}, \mathbf{G}') f_{n\mathbf{k}-\mathbf{q}} (1 - f_{n'\mathbf{k}}) \times \left[ \frac{1}{\omega + \varepsilon_{n\mathbf{k}-\mathbf{q}} - \varepsilon_{n'\mathbf{k}} + i0^+} - \frac{1}{\omega + \varepsilon_{n'\mathbf{k}} - \varepsilon_{n\mathbf{k}-\mathbf{q}} - i0^+} \right]. \quad (8)$$

As the numerical integration of  $\epsilon^{-1}$  in Eq.(5) would require the inversion of Eq.(7) for many frequency points, **yambo** adopts the plasmon-pole approximation (PPA) for the GW self-energy [12]. In the PPA the  $\epsilon^{-1}$  function is approximated with a single pole function

$$\epsilon_{\mathbf{G}\mathbf{G}'}^{-1}(\mathbf{q}, \omega) \approx \delta_{\mathbf{G}\mathbf{G}'} + R_{\mathbf{G}\mathbf{G}'}(\mathbf{q}) \left[ (\omega - \Omega_{\mathbf{G}\mathbf{G}'}(\mathbf{q}) + i0^+)^{-1} - (\omega + \Omega_{\mathbf{G}\mathbf{G}'}(\mathbf{q}) - i0^+)^{-1} \right], \quad (9)$$

and the residuals  $R_{\mathbf{G}\mathbf{G}'}$  and energies  $\Omega_{\mathbf{G}\mathbf{G}'}$  are found by imposing the PPA to reproduce the exact  $\epsilon^{-1}$  function at  $\omega = 0$  and  $\omega = iE_{\text{PPA}}$ , with  $E_{\text{PPA}}$  being a suitable user-defined parameter.

Using Eq. 2 and assuming  $f_{n\mathbf{k}}$  to be either 1 or 0 we have that:

$$(\omega - \varepsilon_{n\mathbf{k}}) G_{n\mathbf{k}}(\omega) = 1 + [\Sigma_{n\mathbf{k}}(\omega) - V_{n\mathbf{k}}^{\text{xc}}] G_{n\mathbf{k}}(\omega). \quad (10)$$

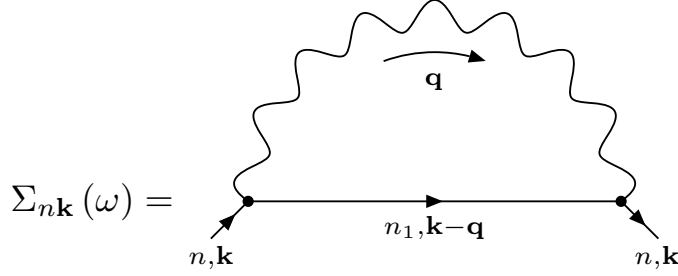


Fig. 1. Diagrammatic representation of the GW approximation for the self-energy operator.

The key approximation is now to take the first order Taylor expansion of the self-energy around  $\varepsilon_{n\mathbf{k}}$  (Newton approximation) in order to get

$$G_{n\mathbf{k}}(\omega) \approx Z_{n\mathbf{k}} \left[ \frac{f_{n\mathbf{k}}}{\omega - E_{n\mathbf{k}}^{QP} - i0^+} + \frac{1 - f_{n\mathbf{k}}}{\omega - E_{n\mathbf{k}}^{QP} + i0^+} \right], \quad (11)$$

with

$$E_{n\mathbf{k}}^{QP} = \varepsilon_{n\mathbf{k}} + Z_{n\mathbf{k}} [\Sigma_{n\mathbf{k}}(\varepsilon_{n\mathbf{k}}) - V_{n\mathbf{k}}^{\text{xc}}], \quad (12)$$

$$Z_{n\mathbf{k}} = \left[ 1 - \left. \frac{d\Sigma_{n\mathbf{k}}(\omega)}{d\omega} \right|_{\omega=\varepsilon_{n\mathbf{k}}} \right]^{-1}. \quad (13)$$

Eqs. (12–13) constitute the QP approximation [12].

It is important to note, at this stage, that by including explicitly the electronic occupations  $f_{n\mathbf{k}}$ , **yambo** can be equally applied to semiconductors, insulators and metals. In the latter case, however, the plasmon-pole approximation can be questionable when some of the valence orbitals are spatially localized (like in  $d$  or  $f$  metals) [13]. Nevertheless for metals in general the RPA is an excellent approximation to the calculation of optical properties, as the efficient screening occurring at the Fermi surface prevents the formation of excitonic states.

## 2.2. Optical properties: the Bethe–Salpeter equation

The evaluation of the response function  $\chi$  makes it possible to calculate the macroscopic dynamical dielectric function  $\epsilon_M$  and polarizability  $\alpha$ . In particular the *macroscopic* dielectric function is defined in terms of the *microscopic* inverse dielectric function as [14]

$$\epsilon_M(\omega) \equiv \lim_{\mathbf{q} \rightarrow 0} \frac{1}{\left[ \epsilon(\mathbf{q}, \omega)^{-1} \right]_{\mathbf{G}=0 \mathbf{G}'=0}}, \quad (14)$$

where  $\epsilon$  is the matrix in the space of reciprocal vectors  $\mathbf{G}$  defined in Eq. (6). Equation (14) implies that, in general, one cannot take the simple spatial macroscopic average of the dielectric function [14] since the charge redistribution induced by the interaction with light induces, in turn, the formation of local microscopic fields—the local field effects. Such effects are particularly important in nanoscale materials where confinement induces the formation of microscopic fields that counteract the external applied perturbation [3]. Similarly the dynamical polarizability of a zero-dimensional electronic system is defined as

$$\alpha(\omega) = -\frac{\Omega}{4\pi} \lim_{\mathbf{q} \rightarrow 0} \frac{1}{q^2} \chi_{\mathbf{G}=0 \mathbf{G}'=0}(\mathbf{q}, \omega), \quad (15)$$

where  $\Omega$  is the unit cell volume.

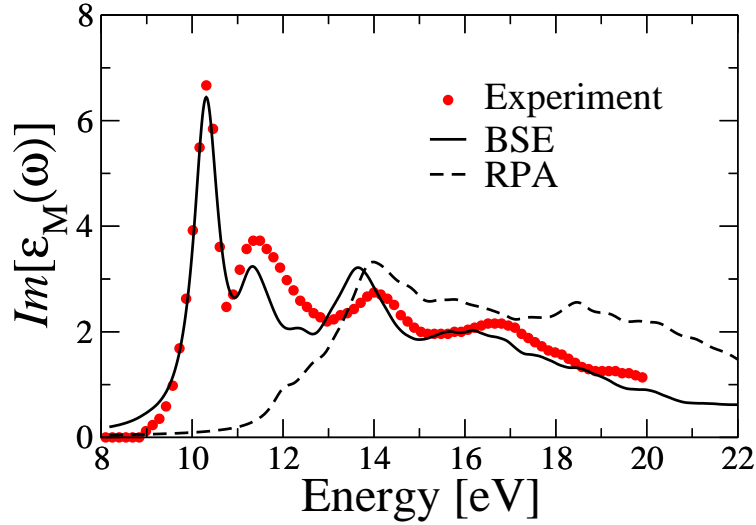


Fig. 2. The calculated absorption spectra of solid SiO<sub>2</sub> within the RPA and through solving the BS equation are compared with the experimental curve. Calculations taken from Ref. [15], experiment from Ref. [16].

The RPA to Eqs.(14,15) is often inadequate to describe the electronic correlations occurring in the response function. In practical applications the RPA does not yield optical absorption spectra in good agreement with experiments for several insulating and metallic systems [3]. For example, in the case of SiO<sub>2</sub>, this discrepancy has led to extensive debates over the past forty years about the nature of the four well-defined peaks observed in the experiment (See Fig. 2). The reason for the poor performance of the RPA is that the response function  $\chi$  measures the change in the electronic density induced by the external applied potential. In a noninteracting system the RPA for  $\chi$  is exact, but self-energy corrections modify the electronic density and, consequently, the RPA approximation is not valid anymore. Therefore, an estimation of the importance of corrections to the RPA can be obtained by looking at the value of the gap correction. The larger the gap, the less adequate is the RPA. The gap of SiO<sub>2</sub>, indeed, is  $\sim 10$  eV and the RPA is not even qualitatively correct.

The drawbacks of the RPA are solved by using a more elaborate equation of motion for  $\chi$  that takes into account the effect of electron–electron correlations. This is the BS equation [11] that can be introduced by using the electron–hole (e–h) Green’s function  $L$ . First we note that the noninteracting  $\mathbf{q} = 0$  response function, Eq.(8), can be rewritten in terms of the noninteracting e–h Green’s function  $L^0$ :

$$\lim_{\mathbf{q} \rightarrow 0} \chi_{\mathbf{G}\mathbf{G}'}^0(\mathbf{q}, \omega) = -i \sum_{nn'\mathbf{k}} \lim_{\mathbf{q} \rightarrow 0} [\rho_{n'\mathbf{k}}^*(\mathbf{q}, \mathbf{G}) \rho_{n\mathbf{k}}(\mathbf{q}, \mathbf{G}')] L_{nn'\mathbf{k}}^0(\omega). \quad (16)$$

To avoid the inversion of Eq.(14), we define a new interacting polarization [3] such that  $\epsilon_M(\mathbf{q}, \omega) \equiv 1 - v(q) \bar{\chi}_{\mathbf{G}=0 \mathbf{G}'=0}(\mathbf{q}, \omega)$ . This function defines a corresponding e–h Green’s function  $\bar{L}$ :

$$\lim_{\mathbf{q} \rightarrow 0} \bar{\chi}_{\mathbf{G}\mathbf{G}'}(\mathbf{q}, \omega) = -i \sum_{nn'\mathbf{k}} \sum_{mm'\mathbf{k}'} \lim_{\mathbf{q} \rightarrow 0} [\rho_{n'\mathbf{k}}^*(\mathbf{q}, \mathbf{G}) \rho_{m'\mathbf{k}'}(\mathbf{q}, \mathbf{G}')] \bar{L}_{mm'\mathbf{k}'}^{nn'\mathbf{k}}(\omega). \quad (17)$$

The BS equation is an equation for  $\bar{L}$ , obtained by performing a second iteration of Hedin’s equation [11]

$$\bar{L}_{mm'\mathbf{k}'}^{nn'\mathbf{k}}(\omega) = L_{nn'\mathbf{k}}^0(\omega) \left[ \delta_{nm} \delta_{n'm'} \delta_{\mathbf{k}\mathbf{k}'} + i \sum_{ss'\mathbf{k}_1} \Xi_{ss'\mathbf{k}_1}^{nn'\mathbf{k}} \bar{L}_{ss'\mathbf{k}_1}^{mm'\mathbf{k}'}(\omega) \right]. \quad (18)$$

The BS equation naturally takes into account the electron–hole interaction in the response function as shown schematically in Fig. 3. The matrix  $\Xi_{ss'\mathbf{k}_1}^{nn'\mathbf{k}} = W_{nn'\mathbf{k}} - 2\bar{V}_{nn'\mathbf{k}}$  is the kernel of the BS equation composed of a direct electron–electron scattering term ( $W$ ) plus an exchange interaction ( $\bar{V}$ ). Both  $W$  and  $\bar{V}$  are integrals of Bloch functions

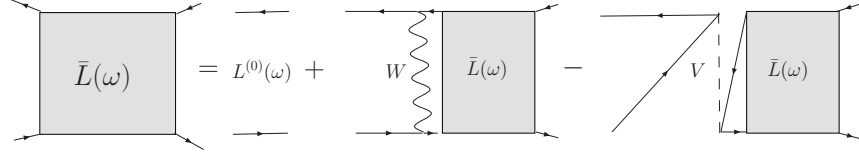


Fig. 3. Diagrammatic representation of the BS equation.

$$W_{ss'\mathbf{k}_1}^{nn'\mathbf{k}} = \frac{1}{\Omega N_q} \sum_{\mathbf{G}\mathbf{G}'} \rho_{ns}(\mathbf{k}, \mathbf{q} = \mathbf{k} - \mathbf{k}_1, \mathbf{G}) \rho_{n's'}^*(\mathbf{k}_1, \mathbf{q} = \mathbf{k} - \mathbf{k}_1, \mathbf{G}') \epsilon_{\mathbf{G}\mathbf{G}'}^{-1} v(\mathbf{q} + \mathbf{G}'), \quad (19)$$

$$\bar{V}_{ss'\mathbf{k}_1}^{nn'\mathbf{k}} = \frac{1}{\Omega N_q} \sum_{\mathbf{G} \neq 0} \rho_{nn'}(\mathbf{k}, \mathbf{q} = 0, \mathbf{G}) \rho_{ss'}^*(\mathbf{k}_1, \mathbf{q} = 0, \mathbf{G}) v(\mathbf{G}). \quad (20)$$

It is important to observe that the BS equation is a Dyson-like equation that should be inverted at each frequency point. The dimension of the  $\bar{L}$  matrix can be, however, quite large and the inversion of Eq.(18) practically impossible. However, for systems with a gap and at zero temperature the noninteracting e-h Green's function can be rewritten as

$$\Re [L_{nn'\mathbf{k}}^0(\omega)] = i \frac{f_{n'\mathbf{k}} - f_{n\mathbf{k}}}{\omega - \varepsilon_{n\mathbf{k}} + \varepsilon_{n'\mathbf{k}}}. \quad (21)$$

As a consequence it can be shown [3] that the BS equation can be reduced to an eigenvalue problem of the Hamiltonian  $H$ ,

$$H_{mm'\mathbf{k}'}^{nn'\mathbf{k}} = (\varepsilon_{n\mathbf{k}} - \varepsilon_{n'\mathbf{k}}) \delta_{nm} \delta_{n'm'} \delta_{\mathbf{k}\mathbf{k}'} + (f_{n'\mathbf{k}} - f_{n\mathbf{k}}) \left[ 2\bar{V}_{mm'\mathbf{k}'}^{nn'\mathbf{k}} - W_{mm'\mathbf{k}'}^{nn'\mathbf{k}} \right]. \quad (22)$$

The Hamiltonian in Eq. (22) is in general non-Hermitian. Nevertheless **yambo** adopts the standard Tamm-Dancoff approximation [17], in which only e-h pairs at positive energy are considered and the Hamiltonian  $H$  is Hermitian. Finally the dielectric function can be expressed in terms of the eigenstates  $|\lambda\rangle$  and eigenvalues  $E_\lambda$  of  $H$ :

$$\epsilon_M(\omega) \equiv 1 - \lim_{\mathbf{q} \rightarrow 0} \frac{8\pi}{|\mathbf{q}|^2 \Omega N_q} \sum_{nn'\mathbf{k}} \sum_{mm'\mathbf{k}'} \rho_{n'n\mathbf{k}}^*(\mathbf{q}, \mathbf{G}) \rho_{m'm\mathbf{k}'}(\mathbf{q}, \mathbf{G}') \sum_{\lambda} \frac{A_{n'n\mathbf{k}}^\lambda (A_{m'm\mathbf{k}'}^\lambda)^*}{\omega - E_\lambda}, \quad (23)$$

with  $A_{n'n\mathbf{k}}^\lambda = \langle n'n\mathbf{k} | \lambda \rangle$  being the eigenvectors of  $H$ .

In the case of semiconductors the BS approach induces only a minor modification of the absorption spectrum. For wide-gap insulators, instead, the energies  $E_\lambda$  may fall within the single particle gap. In this case the eigenstates of the BS equation are called bound excitons [3]. A typical example is shown in Fig. 2 for the case of solid  $\text{SiO}_2$  [18,15].

### 2.3. Time-dependent density functional theory

Time-dependent density functional theory (TDDFT) [8] is gaining increasing popularity as an efficient tool for calculating electronic excitations in finite systems, thanks to its simplicity and moderate computational cost. In TDDFT the *exact* polarization function satisfies a Dyson-like equation that reads

$$\chi_{\mathbf{G}\mathbf{G}'}(\mathbf{q}, \omega) = \chi_{\mathbf{G}\mathbf{G}'}^0(\mathbf{q}, \omega) + \sum_{\mathbf{G}''} \left[ v(\mathbf{q} + \mathbf{G}'') + f_{xc}(\mathbf{q}, \mathbf{G}, \mathbf{G}'') \right] \chi_{\mathbf{G}''\mathbf{G}'}(\mathbf{q}, \omega). \quad (24)$$

Eq.(24) is similar to Eq.(7) with an important addition, the xc kernel  $f_{xc}$  that accounts for the exchange and correlation effects. The exact form of the xc kernel is unknown, but the TDDFT success relies also in the fact that even using the simplest adiabatic local density approximation (ALDA) for  $f_{xc}$  a good accuracy in the evaluation of optical properties can be obtained [19].

We would like to mention here some common limitations of Eq.(24), associated with the use of plane-waves, when applied to low-dimensional electronic systems. As **yambo** is a plane-wave code, it uses the super-cell

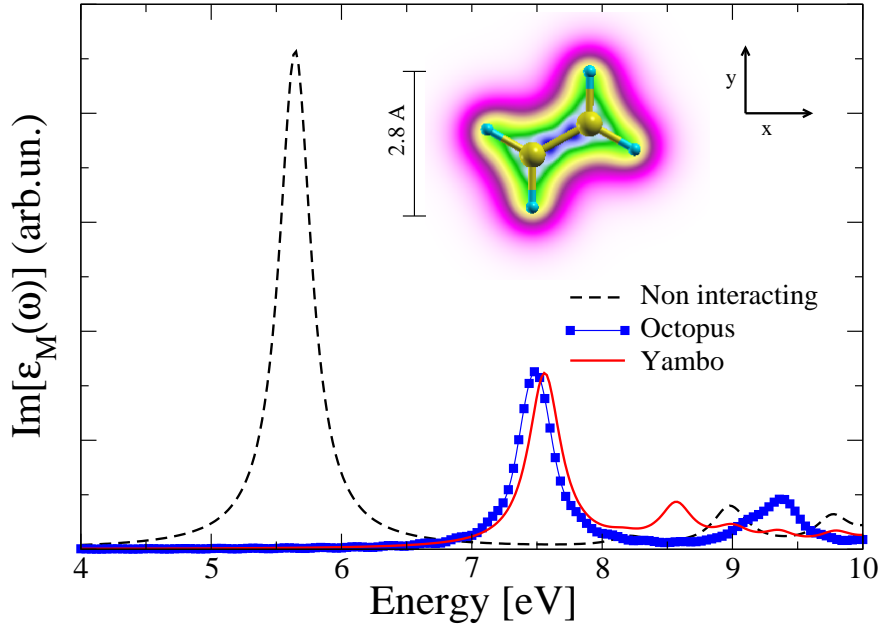


Fig. 4. Calculated photo-absorption spectra at the ALDA level along the  $x$ -direction of an ethylene molecule using either the real-space real-time code `Octopus` [21] and `yambo` in configuration space (see text for detail). Inset: Contour plot of the electronic density of the ethylene molecule placed in a cubic super-cell of side  $10 \text{ \AA}$ .

approach to study small systems like molecules and nanoscale materials. This approach usually leads to two types of problems.

The first of these is the possibility of fictitious interactions between super-cell replicas (images). To treat this problem, `yambo` is capable of removing the long-range tail of Coulomb potentials following the method described in Ref.[20]. The second problem derives from the numerical instability of Eq.(24) that is induced by the presence of large regions of space with vanishing density, as occurs in large supercells (see inset of Fig. 4). Unfortunately, this vanishing density induces some complications to Eq.(24) when  $f_{xc}$  is evaluated at the ALDA level. Indeed, the ALDA kernel is defined by:

$$f_{xc}^{\text{ALDA}}(\mathbf{r}, \mathbf{r}'; t) = \delta(\mathbf{r} - \mathbf{r}') \frac{dv_{xc}^{\text{HEG}}(n)}{dn} \Big|_{n=n(\mathbf{r}, t)}, \quad (25)$$

where  $v_{xc}^{\text{HEG}}(n)$  is the exchange and correlation potential of the homogeneous electron gas. In the region of space with vanishing density we have that  $f_{xc}^{\text{HEG}}(n) \rightarrow \infty$  so that the evaluation of the term involving the  $f_{xc}$  in Eq. (24) cannot be directly calculated in reciprocal space, because the  $f_{xc}^{\text{ALDA}}$  is not well defined. To overcome this problem `yambo` can solve the TDDFT equation within the ALDA in the basis of the e-h pairs, instead of in reciprocal space [Eq. (24)]. In this case the TDDFT equation has the same form of the BS equation, Eq. (18), with the kernel  $\Xi$  given by

$$\Xi_{ss'\mathbf{k}'}^{\text{ALDA}} = -K_{nn'\mathbf{k}}^{\text{ALDA}} - \bar{V}_{nn'\mathbf{k}}, \quad (26)$$

with

$$K_{mm'\mathbf{k}'}^{\text{ALDA}} = 2 \iint d\mathbf{r} d\mathbf{r}' \phi_{n\mathbf{k}}^*(\mathbf{r}) \phi_{n'\mathbf{k}}(\mathbf{r}) f_{xc}^{\text{ALDA}}(\mathbf{r}, \mathbf{r}'; t=0) \phi_{m'\mathbf{k}'}(\mathbf{r}') \phi_{m\mathbf{k}'}^*(\mathbf{r}'). \quad (27)$$

In Fig. 4 we show, as an example, the ALDA dynamical polarizability along the  $x$ -axis of the ethylene molecule. The `yambo` result is compared with a calculation made with the code `octopus`[21] where all the quantities are defined in real-space, and the results are not affected by the presence of regions with zero density and of images due to the super-cell approach. We can see that `yambo` well reproduces the main excitation peak at 7.5 eV, that is composed by bound (localized) electron-hole states[22].



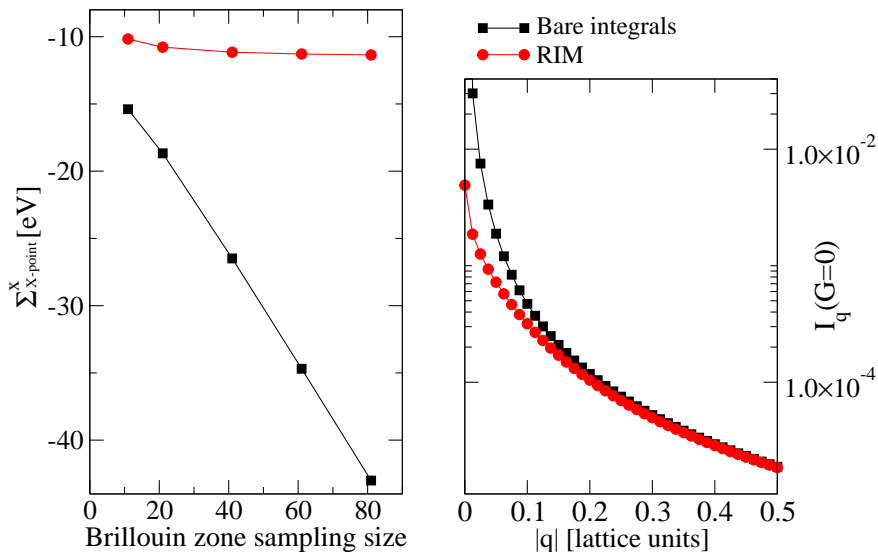


Fig. 5. Left panel: matrix element of  $\Sigma_x$  at the X-point of a *trans*-polyacetylene one-dimensional polymer [23] in function of the number of  $\mathbf{k}$  points used to sample the Brillouin zone, with and without the random integration method. We notice that the RIM removes the divergence of  $\Sigma_x$  as a function of the size of the BZ sampling grid. Right panel:  $I_{\mathbf{q}}(\mathbf{G} = 0)$  integrals as a function of  $|\mathbf{q}|$  for 40  $\mathbf{k}$  Brillouin zone sampling size. The RIM cures the non analyticity of the Coulomb integral near the  $\Gamma$  point. Far from  $\Gamma$  the RIM gradually approaches the bare integral.

### 3. Some numerical aspects

The *yambo* code has been applied to a wide range of materials, from bulk compounds to molecules and nanostructures. As a consequence we have developed several *ad hoc* methods specifically designed to solve physical and numerical problems that can be commonly encountered.

#### 3.1. The random integration method

The definition of the self-energy operator—and of many other quantities—requires an integration in the BZ. In practice this integral is replaced by some suitable grid of points. Let's consider for simplicity only the Hartree–Fock self-energy, given by Eq.(4). Using a finite grid of transferred momenta  $\mathbf{q}$  it reads

$$\Sigma_{n\mathbf{k}}^x \approx -\frac{(2\pi)^3}{N_q \Omega} \sum_{m,\mathbf{q}} \sum_{\mathbf{G}} v(\mathbf{q} + \mathbf{G}) |\rho_{nm}(\mathbf{k}, \mathbf{q}, \mathbf{G})|^2 f_{m(\mathbf{k}-\mathbf{q})}. \quad (28)$$

In approximating  $\Sigma_{n\mathbf{k}}^x$  using a finite grid the key assumption is that the integrand of Eq.(4) must be a smooth function of  $\mathbf{q}$ . While this is generally true for the oscillators  $\rho$  part, this is not so trivial for the Coulomb potential that, indeed, diverges for  $\mathbf{q} \rightarrow \mathbf{0}$ .

Nevertheless, in three-dimensional systems this divergence is not affecting the calculation. In fact, the phase space volume associated with the  $\Gamma$  point reduces as  $|\mathbf{q}|^2$  when  $\mathbf{q} \rightarrow \mathbf{0}$  and the divergence is *de facto* removed. In low-dimensional systems this cancellation holds only if a three-dimensional grid is used. When the Brillouin zone is sampled with lower-dimensional grid instability problems appear in the evaluation of the Coulomb integral. As shown in the right panel of Fig. 5, these instabilities may even grow as a function of the Brillouin zone sampling size. On the other hand using a three-dimensional grid is clearly inconvenient, and more importantly can make the calculations extremely cumbersome.

In order to avoid the use of a three-dimensional sampling in low-dimensional systems *yambo* offers two methods to remove the divergence arising from the Coulomb integrals. The first is based on a cutoff Coulomb technique which is discussed in detail in Ref.[20]. The other is the so-called *random integration method* (RIM) [24]. In the RIM the HF self-energy is rewritten as

$$\Sigma_{n\mathbf{k}}^x \approx - \sum_{m,\mathbf{q}} |\rho_{nm}(\mathbf{k}, \mathbf{q}, \mathbf{G})|^2 f_{m(\mathbf{k}-\mathbf{q})} \int_{R_{\Gamma}} \frac{d\mathbf{q}'}{(2\pi)^3} \sum_{\mathbf{G}} v(\mathbf{q} + \mathbf{q}' + \mathbf{G}). \quad (29)$$

The integral of the Coulomb potential

$$I_{\mathbf{q}}(\mathbf{G}) \equiv \int_{R_{\Gamma}} \frac{d\mathbf{q}'}{(2\pi)^3} \sum_{\mathbf{G}} v(\mathbf{q} + \mathbf{q}' + \mathbf{G}) \quad (30)$$

is evaluated in a region  $R_{\Gamma}$  around the  $\Gamma$  point. Representing as  $R_{\mathbf{q}}$  the region  $R_{\Gamma}$  translated in the general  $\mathbf{q}$  position, this region is chosen in such a way that  $R_{\Gamma} \cup R_{\mathbf{q}_1} \cup R_{\mathbf{q}_2} \dots R_{\mathbf{q}_{N_q}} \equiv BZ$ . The RIM is based again on the uniformity *ansatz* described above, but restricted only to the  $\rho_{nm}$  factors. The  $I_{\mathbf{q}}$  integrals are calculated via a three dimensional Monte Carlo technique [25].

For practical purpose, it is necessary to evaluate only  $I_{\mathbf{q}}(\mathbf{G} = 0)$  because far from the origin the approximation leading to Eq. (28) is still accurate as shown in the right panel of Fig. 5. The importance of the RIM is exemplified in the left panel of Fig. (5) where we show the convergence of  $\Sigma^x$  with respect to the  $\mathbf{k}$ -point sampling at the  $X$  point of a quasi one-dimensional *trans*-polyacetylene polymer.

### 3.2. The Lanczos–Haydock solver of the BS equation

Once the BS (or the TDDFT) Hamiltonian  $H$  [Eq. (22)] has been calculated in the basis of e–h pairs  $|v\mathbf{c}\mathbf{k}\rangle$ , *yambo* offers two options for calculating the corresponding macroscopic dielectric function  $\epsilon_M(\omega)$  and related quantities (optical absorption, electron loss and dynamical polarizability): either via the diagonalization, or via the Lanczos–Haydock (LH) recursion method [26].

With the first option the program diagonalizes  $H$  using the standard BLAS/LAPACK routines [27] to find the eigenvalues  $E_{\lambda}$  and eigenstates  $A_{v\mathbf{c}\mathbf{k}}^{\lambda}$  that define the macroscopic dielectric function, Eq.(23). With the second option Eq. (23) is rewritten as,

$$\epsilon_M(\omega) = 1 - \langle P | (\omega - H)^{-1} | P \rangle, \quad (31)$$

where  $|P\rangle = \lim_{\mathbf{q} \rightarrow 0} \frac{1}{|\mathbf{q}|} |v\mathbf{c}\mathbf{k}\rangle \langle v\mathbf{k} - \mathbf{q} | e^{-i\mathbf{q}\cdot\mathbf{r}} |c\mathbf{k}\rangle$ . Then Eq. (31) is calculated using the LH method [26,28], a general algorithm to compute the matrix elements of the Green's function  $(\omega - H)^{-1}$  applied for the first time to solve the BS equation by Benedict and coworkers [29].

The LH algorithm recursively builds an orthonormal basis  $\{|q_i\rangle\}$  (Lanczos basis) in which  $H$  is represented as a real symmetric tridiagonal matrix,

$$T_j = \begin{pmatrix} a_1 & b_2 & 0 & \dots & 0 \\ b_2 & a_2 & b_3 & & \vdots \\ 0 & \ddots & \ddots & \ddots & 0 \\ \vdots & & b_{j-1} & a_{j-1} & b_j \\ 0 & \dots & 0 & b_j & a_j \end{pmatrix}. \quad (32)$$

The first vector  $|q_1\rangle$  of the Lanczos basis is set equal to  $|P\rangle/\|P\|$ . The next vectors are calculated from the three-term relation

$$b_{j+1}|q_{j+1}\rangle = H|q_j\rangle - a_j|q_j\rangle - b_j|q_{j-1}\rangle. \quad (33)$$

In the Lanczos basis Eq. (31) becomes

$$\epsilon_M^j(\omega) = 1 - \|P\|^2 \frac{1}{(\omega - a_1) - \frac{b_2^2}{(\omega - a_2) - \frac{b_3^2}{\dots}}}. \quad (34)$$

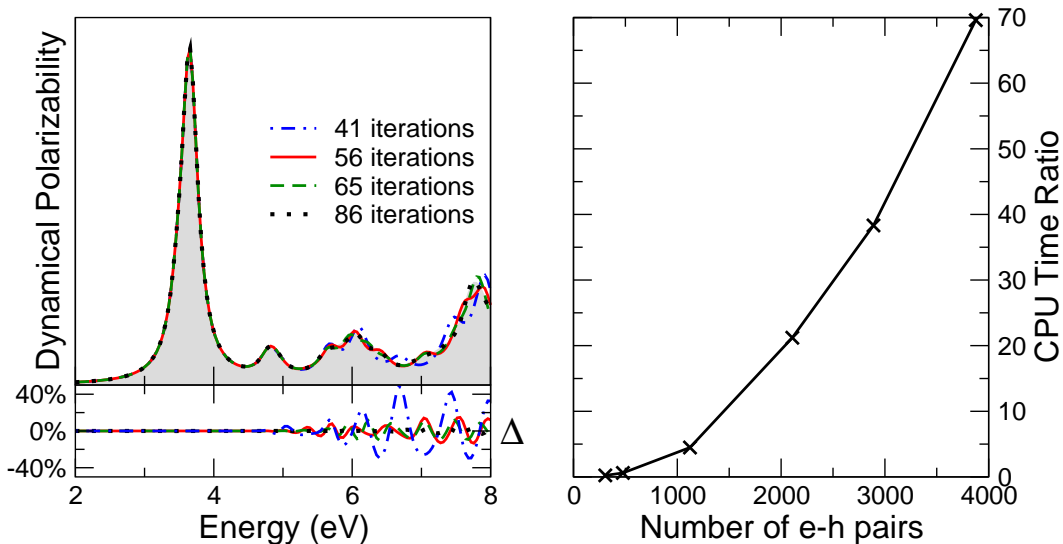


Fig. 6. Left top panel: Dynamical polarizability within the ALDA of the *trans*-azobenzene molecule calculated using either the diagonalization procedure (gray area) or the LH method varying the number of iterations. Left bottom panel: Relative error ( $\Delta$ ) of LH method with respect to the diagonalization varying the number of iterations. Right panel: CPU time ratio between the diagonalization procedure and the LH method (50 iterations) as a function of the e-h pairs included in the Hamiltonian.

At each iteration the program computes a new vector  $|q_{j+1}\rangle$  [Eq. (33)], the matrix elements  $a_j$ ,  $b_{j+1}$ , and thus a better approximation  $\epsilon_M^j$  for  $\epsilon_M$  from Eq. (34). The LH iteration procedure stops when the difference  $|\epsilon_M^j - \epsilon_M^{(j-1)}|$  in the given range of frequencies is smaller than a user-defined threshold.

In practice when interested in a finite range of frequencies one needs a number of iterations  $k$  much smaller than the dimension  $N$  of the Hamiltonian (corresponding to number of e-h pairs included in Eq. 22) to get an accurate  $\epsilon_M(\omega)$ . In the left panel of Fig. 6 this is exemplified for the dynamical polarizability calculated within the ALDA of the *trans*-azobenzene molecule:  $k \approx 50$  is enough for getting an accurate spectrum up to 6 eV, with  $N \approx 4000$ . As a consequence, the LH method [ $O(kN^2)$  floating point operations] is usually much faster than the diagonalization procedure [ $O(N^3)$  floating point operations]. This is clearly shown in the right panel of Fig. 6: already for  $N \approx 1000$  the LH method starts to be more convenient, and for  $N \approx 4000$  it is about 70 times faster than the diagonalization procedure. The LH method is also more convenient in terms of memory since, in contrast with the diagonalization, only three vectors at a time need to be stored. Furthermore, the whole procedure has been efficiently parallelized in **yambo**. The LH algorithm is, therefore, the recommended method in **yambo** for the computation of the macroscopic dielectric function and related quantities, while the diagonalization should be used when the eigenvalues and eigenvectors of  $H$  are explicitly needed, as for example for plotting the excitonic wavefunction via the post-processing tool **ypp**.

#### 4. Overview of the software

The structure of the **yambo** package can be separated into a number of stages, schematically depicted in Fig. 7. In the preliminary stage (I), a C/Fortran90 driver passes control to the main **yambo** executable, or to the data converters (**a2y**, **p2y**, **e2y**). The purpose of the latter is to generate the core *databases* that contain the ground state data necessary for starting the code. A mostly procedural data initialization stage (II) follows, where some general-purpose databases are prepared for later use. The main physical calculations are performed in the third stage (III). Finally, databases created by **yambo** can be further manipulated using the post-processing tool **ypp** in a fourth stage (IV).

Operation of the code follows a series of functionally distinct *runlevels*. The main runlevels are activated by the user via the command-line interface (described in more detail in Sec. 5.2), and others are called

automatically by the code where dependencies are present. Runlevels have a modular structure, in the sense that each one performs specific physical tasks and terminates (in most cases) with the creation of one or several databases written onto disk. These database files may then be accessed by different runlevels. Runlevels may be skipped in subsequent runs if a database is found that is compatible with the user requirements on execution. A more thorough discussion of the databases, and the `yambo` I/O in general, can be found in Sec. 5.3.

The main runlevels are now described in more detail.

Stage I:

- (i) C driver: governs the actions taken by the rest of the code. `yambo` uses a standard `getopt` function [30] to parse the command line. This function is called by all executables to acquire the user-defined options passed at the command line. The syntax is described briefly in Sec. 5.2.
- (ii) Data import/converter: the ground-state electronic structure of the system to be studied is imported from ground state codes (see Sec. 5.1), and converted into the core database files.

Stage II:

- (i) User input: if command line options were added in Stage I, the executable acts as an input file generator. On execution, the code reads default values for input parameters from existing databases and updates the values in the input file, after which the code terminates.
- (ii) Data initialization: reorders  $\mathbf{G}$ -vectors into spherical shells, calculates Fermi level and electronic occupations, sets up energy grids.
- (iii) Brillouin-zone sampling: expands  $\mathbf{k}$ -points to full BZ, generates  $\mathbf{q}$ -point meshes, checks on uniformity of grids.

Stage III:

- (i) Hartree-Fock/Vxc: calculates the matrix elements of the Hartree-Fock exchange self-energy and of the DFT potential corresponding to the type of functional used in the ground state code run.
- (ii) Screening: calculates static and dynamical inverse dielectric functions, for use in the evaluation of the GW self-energy and of the BS/TDDFT kernel.
- (iii) Quasiparticle: calculates quasiparticle corrections to the Kohn–Sham band structure within the GW approximation.
- (iv) Linear response: optical properties within RPA and ALDA with and without local field effects.
- (v) Bethe–Salpeter/TDDFT: creation of the BS/TDDFT Hamiltonian and subsequent diagonalization using LAPACK routines or via Lanczos–Haydock iterative procedure.

Stage IV:

- (i) Post-processing: contains routines for creating  $\mathbf{k}$ -point grids, analyzing single-particle and excitonic wavefunctions and plotting the electronic wavefunctions and density.

## 5. Description of the individual software components

### 5.1. Main utilities

As described earlier, the `yambo` package is in fact composed of three separate utilities. The first of these is the set of converters (`a2y`, `p2y` and `e2y`) which generate the `yambo` core databases from the output of other ground state codes. The `a2y` converter imports data from the so-called `KSS` file as generated by the Abinit code[10], while `p2y` imports data written by the Quantum-ESPRESSO/PWscf[9] code in the `iotk` file format[31]. Alternatively, `e2y` can be used to import data from a netCDF formatted file written according to the ETSF file-format specifications[32]. As a set of high-level libraries are available[33] that are capable of reading and writing this format, it is relatively easy to interface `yambo` with other ground state codes.

The main computation tool is the `yambo` executable itself. Depending on the command line options used (see next section), it can act either as an input file generator or as a straightforward serial or parallel executable.

The last utility is the `ypp` post-processor, which is generally used to perform short analysis of pre-calculated databases.

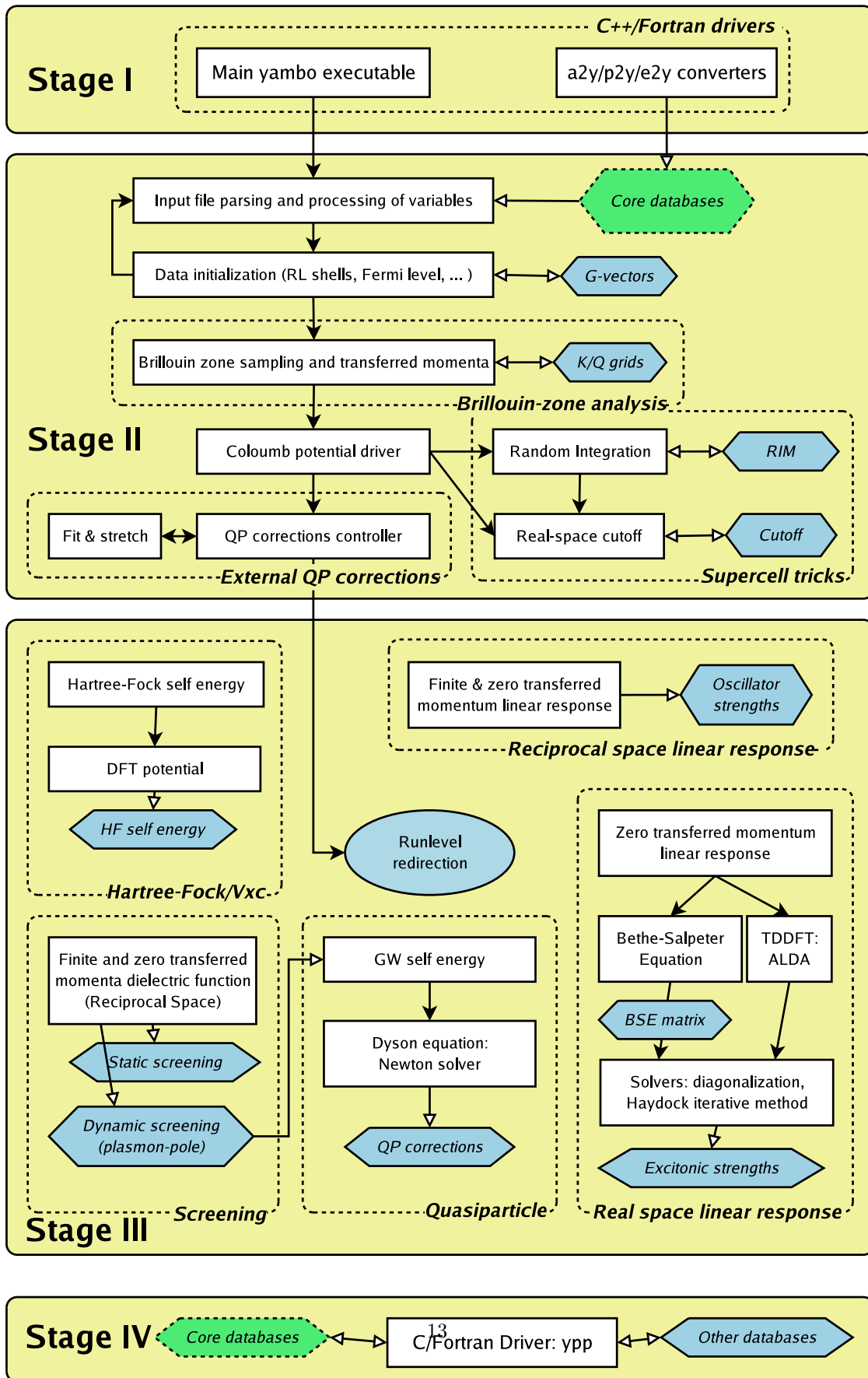


Fig. 7. Simplified schematic chart of the program. Diamond boxes denote some of the most important databases (see text).

## 5.2. Command line interface

Thanks to the C/Fortran driver routine, **yambo** offers a very user-friendly command-line interface for configuring the code at run-time and for creating and editing the main input file. An extended list of options can be displayed by using the `-H` option (see Table 1). **yambo** options can be lowercase and uppercase. Upper case options may be added at run-time to specify input/output directories (`-I/-O`, see next Section), skip the MPI calls (`-N`), create a simple report of the existing database properties (`-D`), and so on. For instance, running

```
yambo -N -I /scratch/tests/silicon-bulk -D
```

will ask for a report of databases in the `/scratch/tests/silicon-bulk` directory, and force the parallel-compiled executable to run in serial.

Lower case options, instead, drive the input file editor. For example,

```
yambo -i -o c -I ~/tests/silicon-bulk
```

will generate an input file (the default being `yambo.in`) that can be used to run the initialization steps (`-i`) and calculate linear response optics at the RPA level (`-o c`). A useful feature of the code is that default values for parameters are suggested based on their values in the most relevant database, if a value is not already present in the input file. Hence if 500 bands are written in the core databases, **yambo** will suggest a range of 1–500 bands for calculating the noninteracting response function.

Since **yambo** offers a huge range of tunable parameters, some of which are quite technical, it would be quite daunting for an average user to face the full list of parameters when running the code. Hence, an input-file verbosity flag (`-V`) lets the user decide how detailed the input file is to appear (the remaining parameters are set to their default values). After checking the existing databases and input files, **yambo** invoked in this way will redirect the user to edit the newly-created `yambo.in` file.

The C parser used by **yambo** to process the input files is taken from the **octopus** [21] code.

## 5.3. I/O: the yambo databases

Files created and accessed by **yambo** are classified according to their purpose and identified by a specific prefix:

- (i) Static database files (prefix `s.`, otherwise known as the core databases) are generated in Stage I (see Fig. 7) by the `a2y`, `p2y` and `e2y` converters. They contain the information concerning the geometry, basis set, wavefunctions and energies, etc.
- (ii) Stable database files (prefix `db.`) are created by **yambo** at run-time, usually in Stage II. They are generally created once and used to store intermediate data designed to be re-read during subsequent executions.
- (iii) Job-dependent database files (prefix `db.`) are also created at run-time but hold information that is usually specific to a particular runlevel (Stage III).
- (iv) Output files (prefix `o.`) are usually created at the end of certain Stage III runlevels and are intended for human use (e.g. suitable for plotting or inspection).

If the netCDF libraries [34] have been configured for use, these database prefixes are further prefixed by `n`, e.g. `ndb.kindx` is the netCDF formatted version of `db.kindx`, the database containing the **k/q**-point grids. Users are strongly advised to use netCDF-linked executables, as the functionality of the code is enhanced. In addition there are auxiliary run-time report files (prefix `r.`) containing the run-time log information, while standard output can be redirected onto disk (prefix `l.`).

Creation of each database is controlled by its own particular Fortran subroutine, e.g. `src/io/ioQP.F` creates the database of QP corrections `db.QP`. However, the actual writing of data is performed at a low level by some common modules, in order to minimize problems associated with portability. Some of the most

yambo	a2y/p2y/e2y	ypp
-h Short Help	-h Short Help	-h Short Help
-H Long Help	-H Long Help	-H Long Help
-J <opt> Job string identifier	-N Skip MPI initialization	-J <opt> Job string identifier
-V <int> Input file verbosity	-F <opt> Input file name/prefix	-F <opt> Input file
-F <opt> Input file	-O <opt> Output directory	-I <opt> Core I/O directory
-I <opt> Core I/O directory	-S DataBases fragmentation	-O <opt> Additional I/O directory
-O <opt> Additional I/O directory	-a <real> Lattice constants factor	-C <opt> Communications I/O directory
-C <opt> Communications I/O directory	-t Force no TR symmetry	-N Skip MPI initialization
-N Skip MPI initialization	-y Force no symmetries	-S DataBases fragmentation
-D DataBases properties	-w Force no wavefunctions	-k K-grid generator
-S DataBases fragmentation		-e <opt> Excitons [(s)ort,(a)mplitude]
-i Initialization		-p <opt> Plot [(e)xciton,(d)ensity,(w)aves]
-o <opt> Optics [opt=(c)hi/(b)se]		-f Free hole position [excitonic plot]
-t <opt> The TDDFTs [opt=(a)LDA/(l)RC]		
-c Coulomb interaction		
-x Hartree-Fock Self-energy and Vxc		
-b Static Inverse Dielectric Matrix		
-p <opt> GW approximations [opt=(p)PA]		
-y <opt> BS equation solver [opt=h/d]		

Table 1

Command line options for the various `yambo` tools.

important databases and their respective runlevels are indicated in Fig. 7 as diamond-shaped boxes.

In order to treat systems with large memory or disk requirements `yambo` offers the capability of fragmenting the larger databases into chunks (`-S`). This functionality is most frequently utilized in the splitting of the ground-state wavefunction files according to  $\mathbf{k}$ -points and/or bands, and in the division of the Bethe–Salpeter Hamiltonian according to the  $\mathbf{k}$ -point index.

By default, all databases are stored in the subfolder `./SAVE` of the working directory. More specific control of I/O directories may be accessed through the various uppercase command line options. For instance, it is common to store the static databases in a ‘core’ directory (`yambo -I COREPATH`), so that they can be shared by different processes. Dynamically-created databases can then be placed elsewhere (`yambo -O OTHER`). Furthermore, users may organize their work better according to a “job string” identifier (`yambo -J JOBNAME`), so that databases and output files are placed in a subdirectory with a name specified by the user. Finally, long jobs, like the creation or diagonalization of the Bethe–Salpeter Hamiltonian, place intermediate results in a `RESTART` folder, so that the job can be continued following a crash or if cpu time limits are exceeded.

## 6. Installation instructions

`yambo` makes use of the GNU autotools suite (`automake/autoconf/libtool`) for installation. Hence, the standard procedure of

```
./configure
make all
```

should create executables for `yambo`, the `ypp` postprocessor and the basic Abinit converter `a2y` and place them in the `bin/` folder of the `yambo` source directory. Detailed installation instructions are available in the manual, including how to enable the `p2y` and `e2y` converters, how to link with `netCDF`, `BLACS` and `FFTW` libraries, change installation options, and so on. In short, a somewhat complete list of compile-time options can be inspected by running the standard command

```
./configure --help
```

## 7. Running yambo: excitonic effects in bulk silicon

In this section we outline the basic steps involved in a typical production run of `yambo`. Normally one would of course start by creating the core databases by importing the output data of some ground state code (see Sec. 5.1). For the purpose of illustration, however, we have included in the `yambo` source a pre-compiled set of core databases for bulk silicon in the `doc/sample` directory (these `netCDF` formatted databases can be extracted by following the instructions in the `doc/sample/bulk_silicon/README` file).

Once the core databases (`ns.db1`, `ns.wf`) are extracted, running `yambo` in the `doc/sample/bulk_silicon/` directory produces as standard output:

```
> yambo

<---> [01] Job Setup
<---> [02] Input variables setup
<---> [02.01] K-grid lattice
<---> [02.02] RL shells
<---> Shells finder |#####| [100%] --(E) --(X)
<---> [02.03] Input (E)nergies[ev] & Occupations
<---> [03] Transferred momenta grid
<---> X indexes |#####| [100%] --(E) --(X)
<---> SE indexes |#####| [100%] --(E) --(X)
<---> [04] Game Over & Game summary
```

This is the Stage II run that `yambo` enters by default whenever, as in this case, no input file has been specified. The results of this setup run (BZ sampling indexes,  $\mathbf{G}$  vector shells, etc.) are stored in two new database files, `SAVE/ndb.gops` and `SAVE/ndb.kindx`, that are to be re-used in subsequent runs. Besides the two databases, `yambo` writes a report file, `r_setup`, that contains a detailed list of information about the run and the system. Every runlevel generates an appropriate report file.

At this stage we can carry out a more interesting calculation: as an example we will calculate the optical absorption spectra of bulk silicon including excitonic effects. To solve the BS equation we will employ the LH algorithm described in Sec. 3.2. First we create the input with the command-line based user interface. From Table 1 we see that the options to use are

```
> yambo -b -o b -y h
```

This command creates the `yambo.in` input file shown in Table 2 and opens it in the default text editor, `vi`. Note that, by reading the databases generated in the setup run, `yambo` already knows that there are 19 momenta permitted by the BZ sampling, and that 50 bands were calculated in the preceding ground-state run. To perform a test calculation we change some of the values in the input.

– In Eq.(17), we restrict the summation from band 2 to band 6:

```
% BSEBands
  2 | 6 | # [BSK] Bands range
%
```

– In the statically screened interaction we use just 51 RL vectors:

```
BSENGBlk= 51 RL # [BSK] Screened interaction block size
NGsBlkXs= 51 RL # [Xs] Response block size
```



---

optics	# [R OPT] Optics
bse	# [R BSK] Bethe Salpeter Equation.
em1s	# [R Xs] Static Inverse Dielectric Matrix
bss	# [R BSS] Bethe Salpeter Equation solver
BSresKmod= "xc"	# [BSK] Resonant Kernel mode. ('x';'c';'d')
% BSEBands	
1   50	# [BSK] Bands range
%	
BSENGBlk= 1 RL	# [BSK] Screened interaction block size
BSENGexx= 411 RL	# [BSK] Exchange components
% QpntsRXs	
1   19	# [Xs] Transferred momenta
%	
% BndsRnXs	
1   50	# [Xs] Polarization function bands
%	
NGsBlkXs= 1 RL	# [Xs] Response block size
% LongDrXs	
1.000000   0.000000   0.000000 —	# [Xs] [cc] Electric Field
%	
BSSmod= "h"	# [BSS] Solvers 'h/d/i/t'
% BEnRange	
0.00000   10.00000   eV	# [BSS] Energy range
%	
% BDmRange	
0.10000   0.10000   eV	# [BSS] Damping range
%	
BEnSteps= 100	# [BSS] Energy steps
% BLongDir	
1.000000   0.000000   0.000000	# [BSS] [cc] Electric Field
%	

---

Table 2

yambo input file needed to perform a calculation of the optical properties of bulk silicon including excitonic effects (see text).

- As the LH method is very fast we increase the number of points on the frequency axis by setting `BEnSteps=1000`. Moreover, to mimic the experimental width of the  $E_1$  and  $E_2$  peaks, we set

```
% BDmRange
0.02000 | 0.8000 | eV # [BSS] Damping range
%
```

Calling `yambo` again, without command line options, will start the calculation, which should last for some minutes. The progress of the calculation (including expected/elapsed time for each time-consuming operation) can be followed from the standard output, or in case of background execution, read from the `l_optics_bse_em1s_bss` log file.

At the end of the run several new files appear in the `SAVE` folder: the dielectric function `ndb.em1s`, the

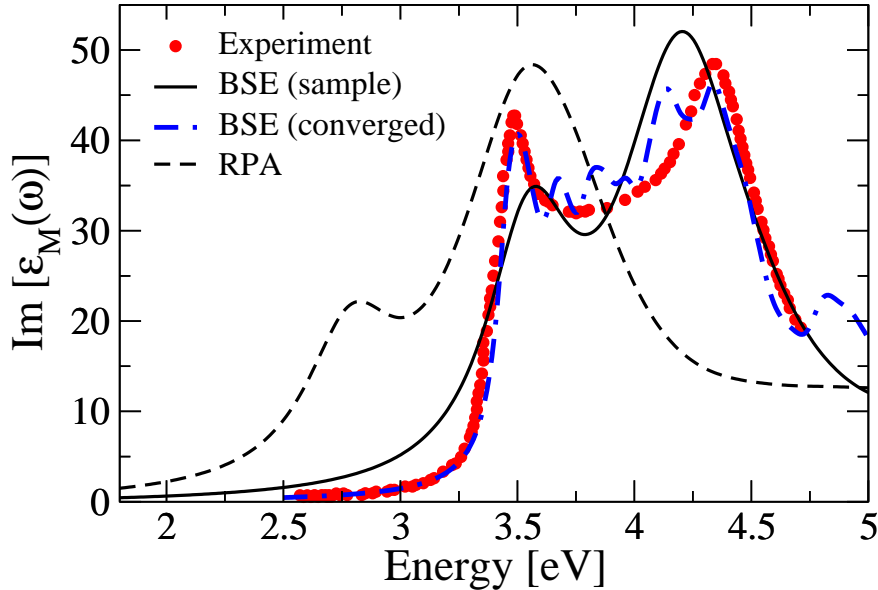


Fig. 8. Optical spectrum of bulk silicon. The result of the sample run described in the text is compared with a more converged calculation [38] and with the experiment [35]. Note that the result of the sample run has been red-shifted by 1 eV to simulate the correct QP gap that, instead, is calculated in the converged spectrum [38].

BS Hamiltonian matrix `ndb.BS_Q1`, and the information needed to restart the LH iterative procedure in `ndb.Haydock_restart`. Furthermore, the run generates two files in the working directory, the report file (`r_optics_bse_em1s_bss`) and the output file (`o_eps_q001-bh`).

The output file contains the calculated spectra (BS and RPA spectra) that can be visualized without further processing with standard plotting tools. Plotting the second versus the first column of the `o_eps_q001-bh` file gives the well-known absorption spectrum of bulk silicon within BSE. The result of the run is shown in Fig. 8, where it is compared with the independent particle (RPA) spectrum (fourth versus the first column of the same file), with the experimental spectrum [35] (included in the `doc/sample/bulk_silicon/experiment.dat` file) and with the result of a more converged calculation [38].

## 8. Appendices

### 8.1. The $\chi^0$ poles accumulation

The noninteracting response function  $\chi^0$  is a key ingredient of the `yambo` code. It enters, for example, in the definition of the RPA dielectric function and of the GW self-energy. Nevertheless the practical evaluation of  $\chi^0$  is often a bottleneck in realistic calculations. The reason is that, as shown in Eq.(8),  $\chi^0$  contains a triple summation over the  $\mathbf{k}$  points and the occupied and empty electronic levels. For systems with a large number of electrons this summation can easily reach millions of elements, that must be multiplied by the number of frequencies.

To provide a tunable and efficient tool to reduce the numerical effort in evaluating  $\chi^0$  `yambo` follows the general idea of the algorithm proposed by Miyake [39] to rewrite  $\chi^0$  as

$$\chi_{\mathbf{G}\mathbf{G}'}^0(\mathbf{q}, \omega) = \frac{2}{\Omega N_k} \sum_p \left[ \sum_{nn'\mathbf{k} \in I_p} \rho_{n'\mathbf{k}}^*(\mathbf{q}, \mathbf{G}) \rho_{n\mathbf{k}}(\mathbf{q}, \mathbf{G}') \right] F_p \left[ \frac{1}{\omega + E_p + i0^+} - \frac{1}{\omega - E_p - i0^+} \right]. \quad (35)$$

In Eq. (35) the  $I_p$  are groups of e-h indexes ( $nn'\mathbf{k}$ ) with similar e-h energies  $\varepsilon_{n'\mathbf{k}} - \varepsilon_{n\mathbf{k}-\mathbf{q}}$ . The latter are approximated with a single pole at  $E_p$  with occupation  $F_p$ . The number of groups created can be controlled by the user by tuning the `CGrdSp` variable in the input file.

The important difference with Eq.(8) is that, in Eq.(35) the evaluation of the oscillators is partially decoupled from the energy dependence. As a consequence by decreasing the groups of e-h pairs it is possible to make the evaluation of  $\chi^0$  almost independent on the number of frequencies.

## 8.2. Oscillator symmetries

The oscillators

$$\rho_{nm}(\mathbf{k}, \mathbf{q}, \mathbf{G}) = \langle n\mathbf{k} | e^{i(\mathbf{q}+\mathbf{G})\cdot\mathbf{r}} | m\mathbf{k} - \mathbf{q} \rangle = \int_{\Omega} d\mathbf{r} \psi_{n\mathbf{k}}^*(\mathbf{r}) e^{i(\mathbf{q}+\mathbf{G})\cdot\mathbf{r}} \psi_{n\mathbf{k}-\mathbf{q}}(\mathbf{r}) \quad (36)$$

appear in almost all the quantities calculated in `yambo`. They are evaluated using efficient Fast Fourier Techniques (FFT) [40]. Nevertheless `yambo` uses symmetry arguments to reduce the number of calls to the FFT interface.

If we specify the symmetry operation by rewriting a general point in the BZ as  $\mathbf{k} = R\mathbf{k}_{IBZ}$ , with  $\mathbf{k}_{IBZ}$  defined in the irreducible wedge of the BZ, Eq.(36) reads

$$\rho_{nm}(\mathbf{k}, \mathbf{q}, \mathbf{G}) = \int_{\Omega} d\mathbf{r} [e^{-iR\mathbf{k}_{IBZ}} u_{nR\mathbf{k}_{IBZ}}^*(\mathbf{r})] e^{i(\mathbf{q}+\mathbf{G})\cdot\mathbf{r}} [e^{iR'(\mathbf{k}-\mathbf{q})_{IBZ} - i\mathbf{G}_0\cdot\mathbf{r}} u_{mR'(\mathbf{k}-\mathbf{q})_{IBZ}}^*(\mathbf{r})], \quad (37)$$

with  $\mathbf{G}_0$  defined as  $\mathbf{G}_0 = \mathbf{k} - \mathbf{q} - (\mathbf{k} - \mathbf{q})_{IBZ}$ . Hence we find that

$$\rho_{nm}(\mathbf{k}, \mathbf{q}, \mathbf{G}) = \int_{\Omega} d\mathbf{r} u_{nR\mathbf{k}_{IBZ}}^*(\mathbf{r}) e^{i(\mathbf{G}-\mathbf{G}_0)\cdot\mathbf{r}} u_{mR'(\mathbf{k}-\mathbf{q})_{IBZ}}(\mathbf{r}). \quad (38)$$

In case of spatial symmetries (a similar procedure applies to the time-reversal symmetry) we can rewrite the left side rotated wavefunction as  $u_{nR\mathbf{k}_{IBZ}}^*(\mathbf{r}) = u_{n\mathbf{k}_{IBZ}}^*(R^{-1}\mathbf{r})$ , so that

$$\rho_{nm}(\mathbf{k}, \mathbf{q}, \mathbf{G}) = \int_{\Omega} d\mathbf{r} u_{n\mathbf{k}_{IBZ}}^*(\mathbf{r}) e^{iR^{-1}(\mathbf{G}-\mathbf{G}_0)\cdot\mathbf{r}} u_{mR^{-1}R'(\mathbf{k}-\mathbf{q})_{IBZ}}(\mathbf{r}). \quad (39)$$

Finally we notice that the symmetries constitute a group, and, consequently,  $R^{-1}R' = S$ , with  $S$  a symmetry operation. Thus, at difference with Eq.(36), Eq.(39) depends only on one symmetry index. By using Eq.(39) the computational cost of calculating all the oscillators at a given  $\mathbf{k}$  point is reduced by the number of symmetries in the star of  $\mathbf{k}$ .

## 9. Acknowledgments

This work was partially supported by the FP6 European Network of Excellence Nanoquanta (NMP4-CT-2004-500198). We acknowledge grant support for code development and testing from the CINECA (account `cne2fm2h`) and CASPUR supercomputing centres. We would like to thank Rodolfo Del Sole and Angel Rubio for their active and continuing support towards the development of the code, both as `yambo` and during the time the code was known as `SELF`.

We would also like to thank the people that have contributed in some way to the development of the code: C. Attaccalite, M. Palumbo, M. Gatti, F. De Fausti, M. Bockstedte, L. Wirtz, G. Onida, X. Gonze.

## References

- [1] The European Theoretical Spectroscopy Facility, <http://www.etsf.eu>.
- [2] R. M. Dreizler and E. K. U. Gross *Density Functional Theory*, Springer Verlag Heidelberg (1990).
- [3] G. Onida, L. Reining, and A. Rubio, *Rev. Mod. Phys.*, **74**, 601 (2002), and references therein.
- [4] J. P. Perdew, R. G. Parr, M. Levy, and J. L. Balduz, *Phys. Rev. Lett.* **49**, 1691 (1982); J. P. Perdew and M. Levy, *ibid.* **51**, 1884 (1983).
- [5] See for example, A.A. Abrikosov, L.P. Gorkov, and E. Dzyaloshinskii, *Methods of Quantum Field Theory in Statistical Physics*, (Dover, New York 1975).
- [6] See for example, M. S. Hybertsen and S. G. Louie, *Phys. Rev. B* **34**, 5390 (1986).

- [7] S. Albrecht, G. Onida, and L. Reining. Phys. Rev. B **55**, 10278 (1997). S. Albrecht, L. Reining., R. Del Sole, and G. Onida, Phys. Rev. Lett. **80**, 4510 (1998).
- [8] See, for instance, M.A.L. Marques, C.A. Ullrich, F. Nogueira, A. Rubio, K. Burke and E.K.U. Gross, Lect. Notes Physics, **706** (Springer, Berlin Heidelberg, 2006)
- [9] QUANTUM-ESPRESSO is a community project for high-quality quantum-simulation software, based on density-functional theory, and coordinated by Paolo Giannozzi. See <http://www.quantum-espresso.org> and <http://www.pwscf.org>.
- [10] X. Gonze, J. M. Beuken, R. Caracas, F. Detraux, M. Fuchs, G. M. Rignanese, L. Sindic, M. Verstraete, G. Zerah, F. Jollet, M. Torrent, A. Roy, M. Mikami, Ph. Ghosez, J. Y. Raty and D. C. Allan, Comp. Mat. Sci. **25**, 478 (2002).
- [11] L. Hedin, Phys. Rev. **139**, A796 (1965); J. Phys.: Condens. Matter **11**, R489, (1999); L. Hedin, and S. Lundqvist, 1969, in *Solid State Physics*, edited by H. Ehrenreich , F. Seitz and D. Turnbull (Academic, New York), Vol. 23, p. 1.
- [12] F. Aryasetiawan and O. Gunnarsson, Rep. Prog. Phys. **61**, 237 (1998).
- [13] A. Marini, R. Del Sole and G. Onida, Phys. Rev. B **66**, 115101 (2002); A. Marini, G. Onida and R. Del Sole, Phys. Rev. Lett., **88**, 016403 (2002); A. Marini, G. Onida and R. Del Sole, Phys. Rev. B, **64**, 195125 (2001).
- [14] H. Ehrenreich, *The Optical Properties of Solids*, Academic, New York (1965).
- [15] A. Marini, R. Del Sole, and A. Rubio, Phys. Rev. Lett. **91**, 256402 (2003).
- [16] H. R. Philipp, Solid State Commun. **4**, 73 (1966).
- [17] A. L Fetter and J. D. Walecka *Quantum Theory of many-particle systems* Dover,(2003), p. 565.
- [18] E. K. Chang, M. Rohlfing, and S. G. Louie Phys. Rev. Lett. **85**, 2613 (2000).
- [19] A. Castro, M.A.L. Marques, D. Varsano, F. Sottile and A. Rubio, *Compte Rendus Physique* (2008) in press
- [20] C.A. Rozzi, D. Varsano, A. Marini, E.K.U. Gross and A. Rubio, Phys. Rev. B. **73**, 205119 (2006)
- [21] M.A.L. Marques, A. Castro, G. F. Bertsch, and A. Rubio, Comput. Phys. Commun., **151**, 60 (2003). The code `octopus` is available at <http://www.tddft.org/programs/octopus/>
- [22] The high energy peaks appearing in Fig. 4 correspond to the excitation of unlocalized orbitals whose different description in the `yambo` and `octopus` codes leads to the discrepancies observed in the figure. Nevertheless, these differences can be systematically removed by increasing the dimension of the basis size.
- [23] D. Varsano, A. Marini, and A. Rubio, Phys. Rev. Lett. **101**, 133002 (2008).
- [24] The RIM implemented in `yambo` has been inspired by the work of O. Pulci, G. Onida, R. Del Sole, and L. Reining, Phys. Rev. Lett. **81**, 5374 (1982).
- [25] M. Evans, T. Swartz, *Approximating Integrals Via Monte Carlo and Deterministic Methods* Oxford University Press, USA (2000).
- [26] R. Haydock, in *Solid State Phys.*, **35** 215 (1980) edited by H. Ehrenfest, F. Seitz, and D. Turnbull, Academic Press.
- [27] E. Anderson, Z. Bai, C. Bischof, S. Blackford, J. Demmel, J. Dongarra, J. Du Croz, A. Greenbaum, S. Hammarling, A. McKenney, et al., *LAPACK Users' Guide, Third Edition* SIAM, Philadelphia, (1999).
- [28] M. Cini, *Topics and Methods in Condensed Matter Theory From Basic Quantum Mechanics to the Frontiers of Research* (Springer, Berlin, 2007) p. 313-316.
- [29] L. X. Benedict and E. L. Shirley, Phys. Rev. B **59**, 5441 (1999).
- [30] The GNU C Library, <http://www.gnu.org/software/libc/>.
- [31] `iotk`: Input-Output Toolkit <http://www.s3.infn.it/iotk/> written by Giovanni Bussi (ETHZ and S<sup>3</sup> Modena). For processing the XML formatted `iotk` data, `yambo` makes use of the high-level wrapper routines available in the `qexml.f90` module written by Andrea Ferretti (S<sup>3</sup> Modena).
- [32] X. Gonze, C.-O. Almbladh, A. Cucca, D. Caliste, C. Freysoldt, M. Marques, V. Olevano, Y. Pouillon, M.J. Verstraete. Comput. Mat. Science **43**, 1056–1065 (2008).
- [33] D. Caliste, Y. Pouillon, M.J. Verstraete, V. Olevano, X. Gonze. Comp. Phys. Comm. **179**, 748–758 (2008).
- [34] NetCDF (network Common Data Form) is a set of software libraries to support the creation, access, and sharing of array-oriented scientific data. The key property of the netCDF databases is that they are platform-independent. For more information visit <http://www.unidata.ucar.edu/software/netcdf/>.
- [35] P. Lautenschlager, M. Garriga, L. Viña, and M. Cardona, Phys. Rev. B **36**, 4821 (1987); G. E. Jellison, Jr. and F. A. Modine, *ibid.* **27**, 7466 (1983).
- [36] H. J. Monkhorst and J. D. Pack, Phys. Rev. B **13**, 5188 (1976).
- [37] Zahlenwerte und Funktionen aus Naturwissenschaften und Technik, in Vol. III of Landolt-Bornstein (Springer, New York, 1982), pt. 17a.
- [38] The sample run of the excitonic optical properties of bulk silicon described in Sec. 7 is introduced to briefly illustrate the steps needed to run `yambo` and, more importantly, is conceived to run in a few seconds on a typical PC. This sample run is not supposed to represent a realistic calculation because of the limited sampling of the BZ and because of the use of too few empty bands to perform a converged *GW* calculation. The more converged BSE spectrum shown in Fig. 8 uses 60(2048) points in the irreducible(reducible) wedge of the BZ (which corresponds to a  $8 \times 8 \times 8$  Monkhorst-Pack(MP) [36] grid). The *GW* QP gap is calculated on the same  $8 \times 8 \times 8$  MP grid but shifted to the origin in such a way as to contain the  $\Gamma$  point. The *GW* gap obtained with `yambo` is 1.20 eV, in excellent agreement with the experimental value of 1.17 [37]. We have used a  $181 \times 181$  plasmon-pole dielectric function  $\epsilon_{GG'}$  which includes up to 60 bands. 150 bands, instead, have been included in Eq.( 5). These converged BSE and QP calculations require a total CPU-time of the order of  $\sim 24$  hours. Interested users can download the relevant input files for these more converged calculations directly from the `yambo` web site <http://www.yambo-code.org/publications.html>.

- [39] T. Miyake, and F. Aryasetiawan, Phys. Rev. B **61**, 7172 (2000).
- [40] See for example S. Goedecker, SIAM Journal on Scientific Computing **18**, 1605 (1997); Comp. Phys. Commun. **76**, 294 (1993). M. Frigo and S. G. Johnson, Proceedings of the IEEE 93 (2), 216231 (2005).